Supplementary Information: Dynamic stabilization of the optical resonances of single nitrogen-vacancy centers in diamond

ELECTROSTATIC MODELING

We modeled the electric field produced by the electrode structure in Fig. 1(c) of the main text using the COMSOL MULTIPHYSICS® electrostatics package. The bottom layer of each electrode is composed of 10 nm of Ti, so for simplicity we model the electrodes as being 100-nm thick, composed entirely of Ti. We use a relative permittivity for the diamond substrate $\epsilon_r = 5.1$. The positions of NV1 and NV2 were determined by fluorescence micrographs, as in Fig. 1(d) of the main text.

Based on our simulations, application of 10 V to one electrode (with the other two electrodes grounded) corresponds to an electric field amplitude at the location of NV1 of 0.9, 0.6, and 1.1 MV/m, for V_1, V_2, and $V_{\rm ref}$, respectively. In Fig. S1 we plot the in-plane electric field components on the diamond surface for $\{V_1, V_2, V_{\rm ref}\} = \{10, 0, 10\}$ V.

As a note of caution: this model assumes a perfect dielectric response. In reality the local field is subject to significant deviations due to charge variations introduced by the electrodes or from photoionization [S1]. These deviations do not substantially affect the performance of dynamic ZPL stabilization, since the proportional gain can be adjusted to compensate (see below), but they do play an important role in static tuning. One example is the photo-induced effect that is responsible for the ~ 4 times greater Stark tuning coefficients for strong (2 mW) cw green excitation, compared with weak (~ 60 nW) red excitation, and is discussed in detail in Ref. [S1].

We also observe hysteretic charging effects which alter the static tuning even with very weak ($\lesssim$ 60 nW) red excitation and without applying any green repump. This hysteresis results in a variation of observed tuning coefficients which depends on scan direction, rate, and history. The variation exists even between successive voltage scans as short as 10 s. Overall, the observed tuning coefficients vary by up to a factor of 5, making a measurement of the intrinsic dipole moment of the NV center a difficult task. Using the Stark tuning coefficients for NV1, determined from the ~ 2 hr forward voltage scan in Fig. 3(a) of the main text, the dipole moment is $\{\Delta d_\parallel, d_\perp\} \approx \{4, 5\}$ GHz/MV/m, which is probably correct to within a factor of 2-3. For this calculation the magnitude of the applied electric field and its angle with respect to the NV axis were estimated based on the electrostatic modeling in Fig. S1 and the dependence of NV1 fluorescence intensity on excitation light polarization.

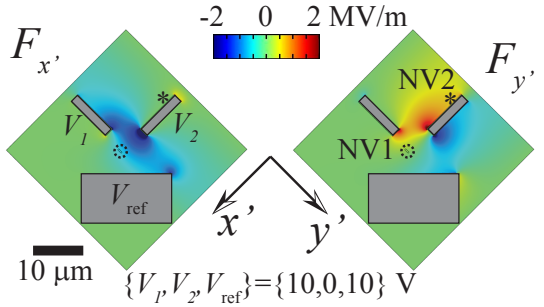

FIG. S1. In-plane electric-field components on the diamond surface, $F_{x',y'}$, for $V_a = 10$ V applied simultaneously to V_1 and $V_{\rm ref}$, with $V_2 = 0$. The locations of NV1 (dashed circle) and NV2 (asterisk) are shown, as in Fig. 1 of the main text. The out-of-plane component $F_{z'} \approx 0$.

REPRODUCIBILITY OF EMISSION SPECTROSCOPY

The reproducibility of Stark emission spectroscopy results was tested by varying the voltage on various combinations of electrodes. Figure S2(a) shows emission spectra while varying the voltage applied to V_1, with $V_2 = V_{\rm ref} = 0$. Despite the continuous voltage tuning, small kinks in the emission lines are observed, particularly following dark frames. During the dark frames of this particular data set, we performed a peak-finding procedure that locates the optical focal position which produces maximum NV emission. The resulting shifts in optical focus may produce small changes in the local field due to photo-induced charge redistribution [S1, S2]. In Fig. 2 of the main text we used a different procedure to maintain optical focus based on continuous feedback using a weak white-light reflection image. This may explain the absence of sharp kinks in the Stark emission spectra in Fig. 2(a).

The inset of Fig. S2(a) shows the low-field spectra, with three emission lines clearly visible. As

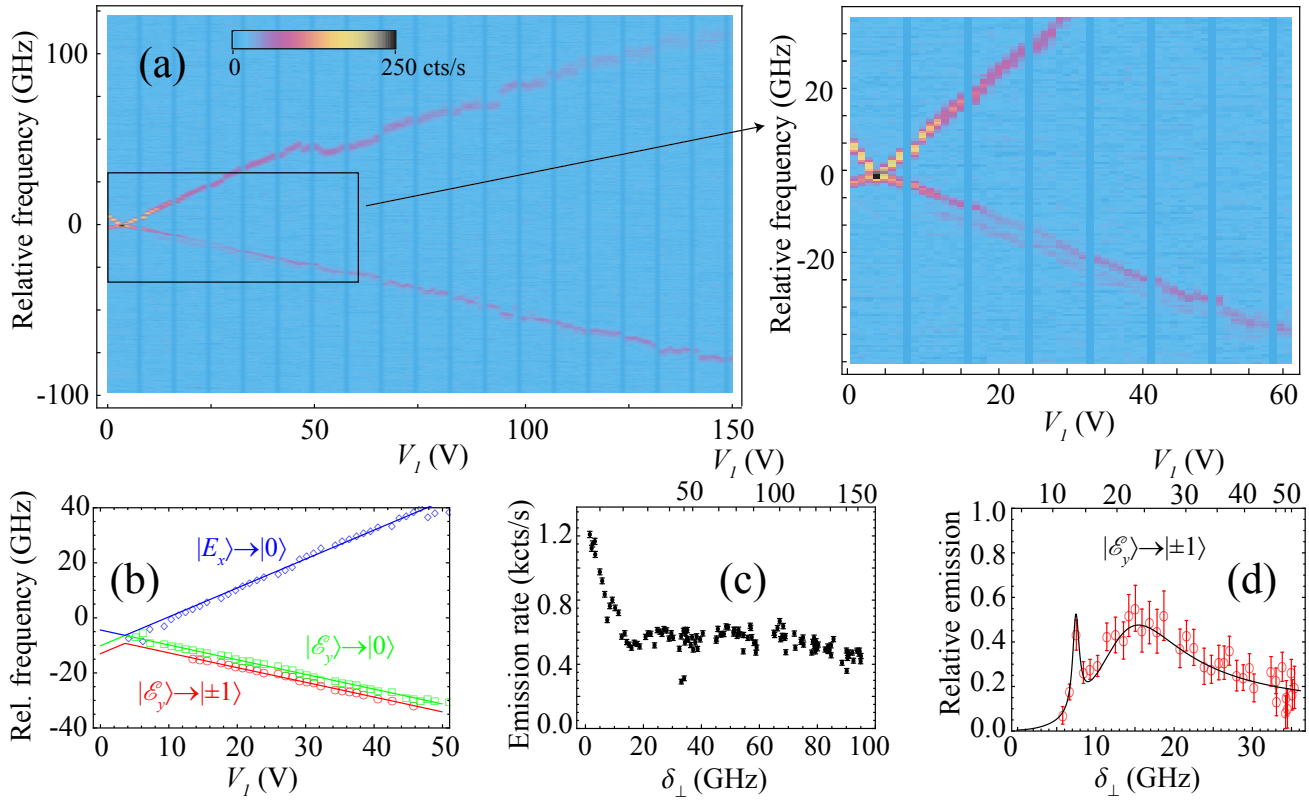

FIG. S2. (a) Stark emission spectra as a function of applied voltage on V_1, with $V_2 = V_{\rm ref} = 0$. Low-field data are displayed on the right. (b) Low-field peak positions determined from Lorentzian fits (symbols) and global fit. Lorentzian fit uncertainty is smaller than the plotted symbols. (c) Total ZPL emission versus $\delta_\perp$. (d) Relative intensity of the $|\mathscr{E}_y\rangle \rightarrow |\pm 1\rangle$ emission line along with fit. The methods for fitting and processing spectra are described in the main text.

in Fig. 2 of the main text, we do not observe $|A_2\rangle \rightarrow |\pm 1\rangle$ emission, indicating ground-state spin polarization, $\mathscr{P}_{GS} \gtrsim 85\%$. Following the procedure outlined in the main text, we fit these spectra [Fig. S2(b)] and found Stark coefficients of $\Delta d_\parallel F_\parallel / V_a = 0.26(2)$ GHz/V and $d_\perp F_\perp / V_a = 0.81(4)$ GHz/V. In Fig. S2(c), the total emission intensity as a function of $\delta_\perp$ is plotted. These data are qualitatively similar to that found in Fig. 2(d) of the main text. In Fig. S2(d), the emission intensity of the $|\mathscr{E}_y\rangle \rightarrow |\pm 1\rangle$ line, relative to the total emission from $|\mathscr{E}_y\rangle$, is plotted versus $\delta_\perp$. Based on the fit, we find $\theta_r = 12(5)^\circ$.

FEEDBACK OPTIMIZATION

The basic feedback protocol is described in the text, and here we outline experimental details. All PLE scans used a ramp waveform with 90% duty cycle. In other words, we scan either the laser frequency or V_{AC} in one direction for 90% of the total scan cycle and the final 10% is devoted to scanning back in the other direction (the "back-scan"). We divide our collected PSB counts into bins of variable size, typically forming 10-50 bins in total. During the backscan of each cycle (denoted with index i), we search for the bin location, b_i, with the maximum counts, C_i. We set a threshold, T, typically corresponding to a count rate of 1 kcts/s, much larger than the background signal off resonance. If $C_i < T$, we apply a green repump pulse for the remainder of the backscan and do not change V_{DC}.

If $C_i \geq T$, we do not apply a repump pulse. Instead, we change V_{DC} by an amount δV_i using the following formula:

$$\delta V_i = G \times (B - \frac{1}{N} \sum_{j=0}^{N-1} b_{i-j}). \qquad \text{(S1)}$$

Here G is a gain factor, N is an integration factor corresponding to the number of cycles used to determine δV_i, and B is the desired peak position. In our experiments, we typically set B to be the bin at the center of each scan. For all of the laser-

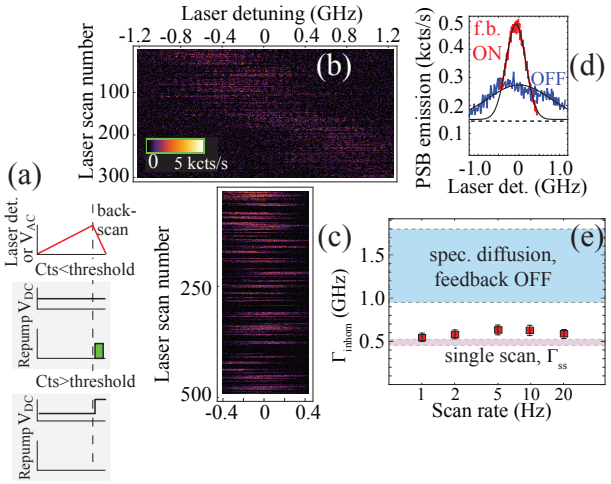

FIG. S3. (a) Timing diagram of the feedback protocol described in the text. (b) PLE spectra for NV2 ($|0\rangle \rightarrow |E_x\rangle$) with $V_a = -4$ V. The scan rate was 1 Hz, and a repump pulse (10 μW, 0.1 s) was applied during every back-scan. (c) PLE spectra for NV2 with feedback applied. The enhanced spectral stability allowed us to reduce the laser-frequency scan range by a factor of four. (d) Sum over the scans in (b) and (c) with, respectively, feedback off (blue) and on (red) along with Gaussian fits (solid black lines) using the mean background of 150 cts/s (black dashed line). (e) Comparison of $\Gamma_{\rm inhom}$ as a function of scan repetition rate. The spectral-diffusion-broadened linewidth (blue shaded region) is the range observed over data sets taken without feedback with 1, 2, 5, 10 and 20 Hz scan rates.

frequency scans in the main text [Fig. 3(d)-(f)], we used $N = 1$ (no integration). For the 0.1-s voltage scans we found that feedback was most efficient using $N = 2$-4. The 100-second portion shown in Fig. 3(g) used $N = 2$. We separately optimize G based on the NV center's Stark tuning coefficients as well as the method and rate of scanning. Figure S3(a) depicts a timing diagram of the feedback routine.

We performed the feedback routine discussed above on the $|0\rangle \rightarrow |E_x\rangle$ transition of NV2 in the NV-doped surface layer sample. Figure S3(b) shows typical PLE spectra when scanning the excitation laser frequency through resonance and applying a repump after each scan. As mentioned in the main text, the average linewidth for single scans, computed using the technique in Ref. [S3], was $\Gamma_{\rm ss} = 0.48(8)$ GHz for NV2. Nonetheless, the ZPL center frequency in Fig. S3(c) drifts over a range significantly larger than $\Gamma_{\rm ss}$ during the 300 s data set.

Figure S3(c) shows PLE spectra under similar conditions as Fig. S3(c) but now with feedback applied. While $\Gamma_{\rm ss}$ remains unchanged, the center-frequency drift is substantially reduced. A figure of merit for the spectral drift of the transition is obtained by summing over many PLE scans and determining the resulting inhomogenous linewidth, $\Gamma_{\rm inhom}$. This figure-of-merit is somewhat different from the histogram technique described in the main text and was employed due to the large single-scan linewidth for this NV center. Figure S3(d) compares the sum of spectra with feedback off [Fig. S3(b)] and on [S3(c)] along with Gaussian fits. Without feedback, we find $\Gamma_{\rm inhom} = 1.8(2)$ GHz $\approx 3.8\Gamma_{\rm ss}$, and with feedback this decreases to 0.54(4) GHz $\approx 1.1\Gamma_{\rm ss}$.

This feedback technique can be applied at significantly higher bandwidth without compromising stability. Figure S3(e) plots $\Gamma_{\rm inhom}$ as a function of scan repetition rate up to 20 Hz. Throughout this range, we find $\Gamma_{\rm inhom} \lesssim 1.3\Gamma_{\rm ss}$. Future improvements could involve ultra-fast correlation measurements to determine the nature of the broad single-scan linewidth [S4].

[S1] L. Bassett, F. Heremans, C. Yale, B. Buckley, and D. Awschalom, Physical Review Letters **107** (2011), 10.1103/PhysRevLett.107.266403.

[S2] H. Bernien, L. Childress, L. Robledo, M. Markham, D. Twitchen, and R. Hanson, Physical Review Letters **108** (2012), 10.1103/PhysRevLett.108.043604.

[S3] K.-M. C. Fu, C. Santori, P. E. Barclay, L. J. Rogers, N. B. Manson, and R. G. Beausoleil, Physical Review Letters **103**, 256404 (2009).

[S4] G. Sallen, A. Tribu, T. Aichele, R. André, L. Besombes, C. Bougerol, M. Richard, S. Tatarenko, K. Kheng, and J.-P. Poizat, Nature Photonics **4**, 696 (2010).